Models for Induction Machines with Magnetic Saturation of the Main Flux Path

Charles R. Sullivan*
Seth R. Sanders
Member, IEEE
Electrical Engineering and Computer Sciences Department
Cory Hall
University of California
Berkeley CA 94720 U. S. A.

Abstract– **A new nonlinear π-model for an induction machine operating in magnetic saturation has been developed. It is based on a magnetic circuit model of a rotor-stator tooth pair, with nonlinear elements representing the saturation in the rotor and in the stator. The model of a tooth pair is extended to a model of the machine by assuming an infinite number of infinitesimal teeth. The model is compatible with the Blondel-Park transformation. Experimental measurements on a wound-rotor machine confirm the new model. Operating conditions for optimal efficiency at high torque levels requiring operation in saturation are computed with the new model.**

I. Introduction

Induction machines are usually modeled with the assumption of linear magnetics. This is a good approximation at low flux levels, but becomes inaccurate at higher flux levels. If a machine is to be operated at flux levels well above its rating, the model must include saturation to be useful. Even for a machine operated at its rating, magnetic saturation may be important if a very accurate model is required.

Operation in magnetic saturation allows an induction machine to produce higher torque than is possible at lower flux levels. Thus in applications where it is important to get high peak power or high peak torque from a small machine, it is necessary to understand how saturation affects the torque and efficiency. If the application calls for a precise speed or position control system, then the effects of saturation on the control system are also important. Other applications in which saturation is important include asynchronous generation and simple six-step speed control systems. In asynchronous generation, machines designed as motors are often used as generators, which results in larger fluxes at the same voltage. Six-step speed control systems, in which the frequency is reduced, but the voltage is kept constant, result in large fluxes at low speeds.

It has been recently noted that saturation effects in smooth air-gap machines can introduce cross-coupling effects that are not predicted by linear models. In a two-axis machine (or model) the current in one winding can affect the flux in the orthogonal winding. The 'cross saturation' model [1, 2, 3, 4, 5, 6] has become the standard method of accounting for these effects. The model is based on the conventional T-model of an induction machine, and the saturation is assumed to be entirely in the mutual inductance, not in the leakage, as shown in Fig. 1. In a two-axis machine model the currents and voltages are vector quantities, and the vector characteristics of the nonlinear mutual inductance give rise to the cross-saturation effects. Although previous authors have carefully derived these vector characteristics from physical models, the overall form of the T-model has merely been postulated by extending a standard linear-magnetics model to include saturation of the mutual path.

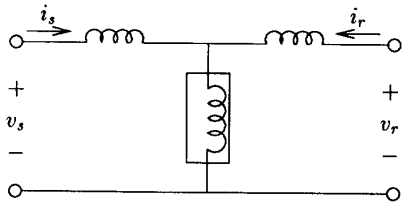

Figure 1: Nonlinear T-model of one phase of a saturating induction machine, with rotor and stator mechanically aligned. Boxed element is nonlinear.

This paper develops a new model, based on a nonlinear magnetic circuit model of the machine. The resulting electric circuit model is a nonlinear π circuit. In the linear-magnetics case, a π-model is equivalent to a T-model. With saturation, however, the two are no longer equivalent. In addition to being more closely based on a physical model of the machine, the new π-model has the advantage of being easier to use in some control and simulation applications [7].

Essential to much conventional analysis and control is the ability to perform a Blondel-Park Transformation, as discussed for the general linear-magnetics case in [8]. The T-model is shown in [5] to allow the transformation. The new π-model is also shown to allow the transformation. In this paper, the π-model is applied to steady-state opera-

*The first author has been supported by an NSF Graduate Fellowship.

0-7803-0768-2/92$03.00 ©IEEE

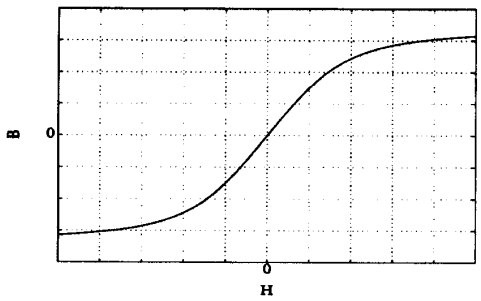

Figure 2: Typical saturation characteristic

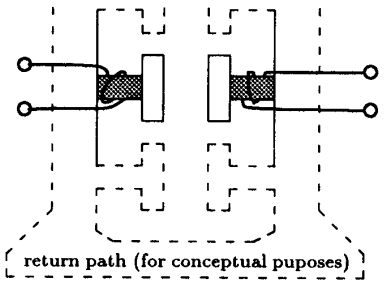

Figure 3: Simplified tooth structure

tion in saturation, and to the analysis of optimal efficiency operation above rated torque. See [7] for details on field-oriented control schemes based on the π-model.

II. Magnetic Circuit Models

To derive the appropriate form for a model of an induction machine in magnetic saturation, we use standard magnetic circuit modeling, augmented by the use of nonlinear reluctances to represent saturating portions of the steel. The B-H characteristic of the steel is assumed to be a single-valued nonlinear monotonic function, generally having a shape such as the curve in Fig. 2. The flux/MMF characteristic of the reluctance element, for simple geometries, is just the B-H characteristic, scaled by cross-sectional area for flux, and by length for MMF. Useful characteristics of this function are that it is invertible, symmetric, and monotonic. We will represent it by $NI = g(\Phi)$, or $\Phi = g^{-1}(NI)$.

Fig. 3 shows the simplified tooth structure for a single pair of teeth in an induction machine. Fig. 4 shows one way of drawing a magnetic circuit model for the tooth pair, making the assumption that the only portions of the steel that saturate are the central legs, shown shaded in Fig. 3.

We proceed with a series of transformations to get to an electrical circuit model. Since the central section of the circuit in Fig. 4 is a linear π circuit, it can be replaced

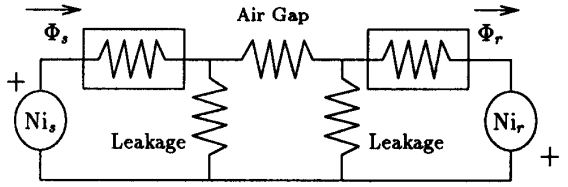

Figure 4: Magnetic circuit of tooth pair. Boxed elements are nonlinear.

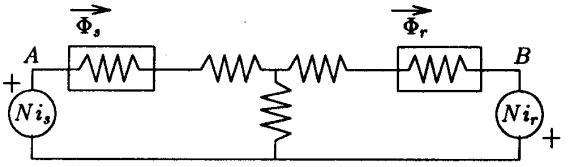

Figure 5: Modified magnetic circuit of a tooth pair with the center π circuit replaced by a T circuit.

by an equivalent T circuit, as shown in Fig. 5. Next we take the dual of the circuit in Fig. 5 to get the circuit in Fig. 6, with flux as the across variable and MMF as the through variable. Scaling by the number of turns[1] we can reformulate the circuit in terms of flux linkages and current. The circuit is then of exactly the same form as Fig. 6, but has scaled elements. The last step in getting an electric circuit is to convert from flux linkage to voltage by differentiating with respect to time. The resistances get replaced by inductances, and the final model for the tooth pair, shown in Fig. 7, results.

As a result of the transformation of the π circuit to a T circuit in moving from Fig. 4 to Fig. 5, the linear inductors in Fig. 7 no longer have direct physical meaning. However, the nonlinear inductors correspond directly to the nonlinear reluctance in the shaded portion of the tooth in Fig. 3. For convenience and clarity, we lump the linear portion of the nonlinear inductors with the parallel inductors, L_s and L_r.

As drawn, the circuit in Fig. 7 could have circulating currents in various loops of inductors. In the linear case these are unobservable, uncontrollable modes. In the nonlinear case, the circulating current would not appear directly at the rotor and stator terminals, yet could affect the apparent nonlinear characteristics of the inductances. There are, however, additional constraints resulting from the magnetic circuit. From Fig. 5, the analogy to Kirchoff's current law requires that the flux through the two stator reluctances be equal, that the flux through the two rotor reluctances be equal, and that the flux through the

[1] We assume for simplicity that the numbers of turns on the rotor and stator are equal. Unequal numbers of turns can be treated by the appropriate scaling.

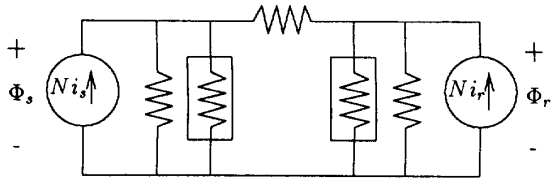

Figure 6: The dual of the modified magnetic circuit.

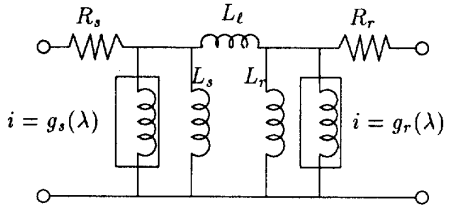

Figure 7: Electric circuit of tooth pair

leakage path be equal to the difference in the rotor and stator fluxes. In Fig. 7, these become the constraints that the flux linkage in L_ℓ must be equal to the difference in flux linkages in L_r and L_s, the flux linkages in $g_s(\cdot)$ and L_s must be equal, and the flux linkages in $g_r(\cdot)$ and L_r must be equal. Note that these constraints would be satisfied automatically by the circuit of Fig. 7, given initial conditions with zero circulating current, but adding the algebraic constraint is advantageous because it reduces the order of the model.

It is useful at this point to consider working backward from a nonlinear T-model to see what magnetic circuit it corresponds to. The result is a magnetic π circuit, as shown in Fig. 8. This might correspond physically to having the air gap replaced by a material with a low saturation flux density. It does not correspond well to any common machine construction.

III. Vector Characteristics of Saturation

To move from the model of a single tooth pair to a model of a symmetric induction machine, we first step back and consider the vector characteristics of a simpler structure, a machine with windings only on the stator. The model of each tooth can then just be a single nonlinear reluctance, described by $g(\Phi) = NI$, where $g(\cdot)$ now includes the linear part of the reluctance. To model this machine, we consider the stator to be constructed of an infinite number of infinitesimal teeth, each with the appropriate number of turns of each phase, according to the sinusoidal distribution. To determine the flux linkage in the windings, we

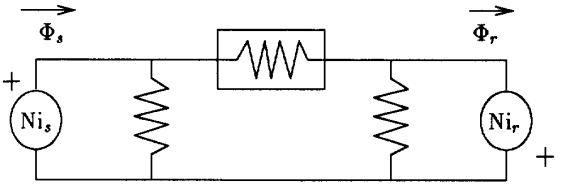

Figure 8: Magnetic circuit that would correspond to the nonlinear T-model of a saturating induction machine.

integrate

$$\vec{\lambda} = \begin{bmatrix} \lambda_d \\ \lambda_q \end{bmatrix} = F^{-1}(\vec{\imath}) \qquad (1)$$
$$= \begin{bmatrix} \int_0^{2\pi} N\cos\theta\, g^{-1}\left(Ni_d\cos\theta + Ni_q\sin\theta\right) d\theta \\ \int_0^{2\pi} N\sin\theta\, g^{-1}\left(Ni_d\cos\theta + Ni_q\sin\theta\right) d\theta \end{bmatrix}.$$

For a given numerical or analytic form of $g^{-1}(\cdot)$, this could be solved explicitly. However, in a typical practical situation, $g^{-1}(\cdot)$ is not known, and is not easy to measure. The function $F(\cdot)$ describes the overall terminal quantities, and so is easier to measure. However, even without measuring either function, we can deduce some characteristics of the function $F(\cdot)$ from the form of (1).

In (1) we are taking the result of applying a nonlinear function $g^{-1}(\cdot)$ to a sinusoid, and extracting the component at the fundamental frequency of the input. This situation has been analyzed extensively in nonlinear control system theory, where it is called *describing function* analysis [9]. Describing function analysis is generally applied to sinusoidal functions of time, but we can apply it just as well to a sinusoidal function of spatial angle in the machine. Describing function analysis is generally an approximate method, because the assumption that the input is a sine wave is usually not exact, and because ignoring all harmonics at the output may also involve some approximation. However, for the analysis of the hypothetical machine with only stator windings and an infinite number of teeth, the method is exact. The input is forced to be a sinusoid by the sinusoidal winding pattern, and the output harmonics are of no consequence, because only the fundamental component contributes to the flux linkage in the sinusoidal windings.

With describing function analysis of functions of time, it can be shown that a memoryless nonlinearity produces no phase shift between the input and output sinusoids. In the machine, spatial independence of $g^{-1}(\cdot)$ is analogous, and the result is that, the phase or direction of the flux linkage vector is the same as the direction of the current vector. The smooth air gap, and identical teeth result in $g^{-1}(\cdot)$ being independent of angle. Thus the magnitude of the output is independent of the phase angle of the input, and depends only on the input amplitude. Hence, the relation between flux and current can be written

$$\vec{\imath} = F(\vec{\lambda}) = f(||\vec{\lambda}||)\frac{\vec{\lambda}}{||\vec{\lambda}||}, \qquad (2)$$

where $f(\cdot)$ is the scalar function relating the magnitude of the input to the magnitude of the output. It has a similar shape to the inverse of the saturation function shown in Fig. 2, but is related to $g(\cdot)$ indirectly through (1). Note that one could consider the quantity $||\vec{\lambda}||/f(||\vec{\lambda}||)$ to be an inductance that varies as a function of $||\vec{\lambda}||$, so that $\vec{\imath} = \vec{\lambda}/L(||\vec{\lambda}||)$. This is the notation used in most discussions of the nonlinear T-model, and is mathematically equivalent. We choose to use the $F(\cdot)$ notation instead, because it makes clear which elements are linear and which are not.

Now we are ready to model an entire machine with rotor and stator windings. Again we consider an infinite number of infinitesimal teeth, but now we use complete tooth pairs. Thus the model for an infinitesimal angular element is as in Figs. 3–7. We can think of this model with an infinite number of teeth as a magnetic circuit, as in Fig. 4 or 5, but with each flux or MMF being a spatial distribution over 2π radians, instead of just a scalar quantity.

The spatial distribution of the MMF between nodes A and B in Fig. 5 is forced by the sinusoidally distributed windings to be sinusoidal. However, the MMF distribution across each circuit element need not be exactly sinusoidal. Nevertheless, we will model the machine by assuming that the MMF across each element is in fact sinusoidal. There are several reasons that this can be expected to be a very good approximation. The rotor and stator saturation characteristics, $g_s(\cdot)$ and $g_r(\cdot)$, each have odd symmetry. If in addition, leakage inductance is low, and the rotor and stator saturation characteristics are similar to each other, the MMF at the center node in Fig. 5 will be, by symmetry, approximately the average of the rotor and stator MMF's. Thus it will be approximately sinusoidal. Furthermore, even if these conditions do not hold, and the MMF at the center node is not exactly sinusoidal, the effect of the harmonics on the result of interest, the fundamental component of the flux through the stator and rotor windings, will be small. This is verified numerically in Section IV.

Note that we are not assuming the flux distribution to be sinusoidal. However, since only the sinusoidal components of the flux distribution appear in the flux linkage, the flux linkage can be represented by a flux linkage vector. This results in an accurate lumped model for the dynamics of the machine as seen from terminal quantities, without explicitly including the flux distribution. The two nonlinear elements are modeled by functions of the form (2), which we we call $F_s(\cdot)$ and $F_r(\cdot)$. These functions represent the saturation characteristics of the saturating portions of all the stator teeth or all the rotor teeth acting together. As before, the linear portions of the nonlinear inductances are lumped with the parallel inductances L_s and L_r, so that $F_s(\cdot)$ so that $F_r(\cdot)$ include only second order and higher terms. For a machine with rotor and stator mechanically aligned, the model can be written,

$$\vec{\imath}_s = F_s(\vec{\lambda}_s) + (\frac{1}{L_s} + \frac{1}{L_\ell})\vec{\lambda}_s - \frac{1}{L_\ell}\vec{\lambda}_r \qquad (3)$$

$$\vec{\imath}_r = F_r(\vec{\lambda}_r) + (\frac{1}{L_r} + \frac{1}{L_\ell})\vec{\lambda}_r - \frac{1}{L_\ell}\vec{\lambda}_s, \qquad (4)$$

and

$$\dot{\vec{\lambda}}_s = \vec{v}_s - \mathbf{R}_s\,\vec{\imath}_s \qquad (5)$$

$$\dot{\vec{\lambda}}_r = \vec{v}_r - \mathbf{R}_r\,\vec{\imath}_r, \qquad (6)$$

where the dot ($\dot{}$) indicates differentiation with respect to time. Due to the symmetry of the machine, the resistance matrices $\mathbf{R_s}$ and $\mathbf{R_r}$ are just the identity multiplied by scalar resistances. This is a vector version of the tooth-pair π circuit in Fig. 7, with the functions $F_s(\cdot)$ and $F_r(\cdot)$ as the nonlinear characteristics of the saturating vector inductors.

To account for the rotor being mechanically located at an angle θ, the rotor quantities are multiplied by $e^{\mathbf{J}\theta}$, where $\mathbf{J}$ is the rotational matrix

$$\mathbf{J} = \begin{bmatrix} 0 & -1 \\ 1 & 0 \end{bmatrix},$$

to get

$$\vec{\imath}_s^{\,s} = F_s(\vec{\lambda}_s^{\,s}) + (\frac{1}{L_s} + \frac{1}{L_\ell})\vec{\lambda}_s^{\,s} - \frac{1}{L_\ell}e^{\mathbf{J}\theta}\vec{\lambda}_r^{\,r} \qquad (7)$$

$$e^{\mathbf{J}\theta}\vec{\imath}_r^{\,r} = F_r(e^{\mathbf{J}\theta}\vec{\lambda}_r^{\,r}) + (\frac{1}{L_r} + \frac{1}{L_\ell})e^{\mathbf{J}\theta}\vec{\lambda}_r^{\,r} - \frac{1}{L_\ell}\vec{\lambda}_s^{\,s}. \qquad (8)$$

The subscript s or r on flux linkage or current (λ or i) indicates stator or rotor quantities. The superscript s indicates that the flux or current is measured in the stator reference frame, and the superscript r indicates coordinates fixed to the mechanical rotation of the rotor. The rotor current equation can be multiplied by $e^{-\mathbf{J}\theta}$ to get

$$\vec{\imath}_r^{\,r} = F_r(\vec{\lambda}_r^{\,r}) + (\frac{1}{L_r} + \frac{1}{L_\ell})\vec{\lambda}_r^{\,r} - \frac{1}{L_\ell}e^{-\mathbf{J}\theta}\vec{\lambda}_s^{\,s}, \qquad (9)$$

where we have taken advantage of the fact that the characteristics of the functions $F_s(\cdot)$ and $F_r(\cdot)$ allow moving a rotation ($e^{-\mathbf{J}\theta}$) inside or outside the function.

IV. Verification of the Model

To verify the model, measurements were made on a 3 hp wound-rotor machine. With the rotor blocked at $\theta = 0$, the rotor and stator were fed from separate three-phase variable autotransformers. A set of 146 data points was taken on a grid of rotor and stator voltages, with the voltages in phase, up to about twice the rated voltage of the machine.

In order to fit the models to this data, it was necessary to use a parameterization of the scalar flux/current relationship, $f(\cdot)$. We selected a function with the general shape of the saturation characteristic in Fig. 2, and with parameters that could be varied to get a good fit. We chose to use the form

$$i = \frac{s_1 - s_2}{(b^{-n} + \lambda^{-n})^{\frac{1}{n}}} + s_2\lambda \qquad (10)$$

where s_1 is the initial slope, s_2 is the final slope, b is the breakpoint, and n is the sharpness of the transition between slopes. As n approaches infinity, the function approaches a piecewise linear function.

A numerical least-squares fit was performed to find the values of these parameters for the nonlinear inductors, and the values of the rotor and stator resistances. For the purposes of comparison, fits for the T-model were also made.

TABLE I
ERROR IN FIT OF π- AND T-MODELS TO MEASURED DATA

	T-model fit to minimize voltage error	π-model fit to minimize current error
Normalized current error	0.192	0.082
Normalized voltage error	0.088	0.103
Maximum rotor or stator current error at any data point	9.98 A	4.45 A

All inductors in both models were allowed to be nonlinear, so as to learn whether approximating the leakage inductance as linear is a good approximation. In order to make the numerical least-squares fit computationally efficient, it was necessary to use different error criteria for the two models. For the π-model, parameters were computed to minimize error in the current predicted by the model for given sets of rotor and stator voltages. For the the T-model, the voltage error was minimized for given currents. For the purpose of comparing the fit of the two models, errors were computed both ways for both models. The rms of the absolute error of all the data points was computed, and divided by the rms of the measured values, to get the normalized error shown in Table I. Also listed is the maximum rotor or stator current error taken over all data points. The π-model fits better than the T-model when evaluated by current error, but the T-model fits slightly better than the π-model when evaluated by voltage error. Current error is likely to be more important, because in the state space equations, the model is used to calculate current from flux. From Table I it appears that overall the π-model has a better fit.

In Figures 9-10, actual rotor currents are compared with rotor currents predicted for the π- and T-models. Current vectors are plotted originating from points representing the magnitude of the rotor and stator voltages. Stator current plots are similar, but rotor current is shown because effects of saturation are more apparent in the rotor. The rotor saturates at a lower flux level, because of its smaller cross-sectional area.

We conclude that, for this machine, both models fit well. We also note that the fit showed that leakage inductance in the π-model is very close to linear. Leakage inductance in the T-model is also close to linear, though this approximation may be less accurate. A fit using parallel resistance to model core loss was also carried out. Since this did not significantly improve the fit, we assume core loss is in fact negligible, for the purpose of fitting an accurate model of machine dynamics in saturation.

In order to verify that the approximation that the MMF distributions are all sinusoidal does not introduce significant errors in the resulting models, we calculate the flux linkage as a function of current for a hypothetical machine. The calculation is done first exactly, and second using the approximation. The hypothetical machine has piecewise linear saturation characteristics for the teeth, because this is expected to be a worst case for producing non-sinusoidal MMF distributions, compared to a more realistic gradual

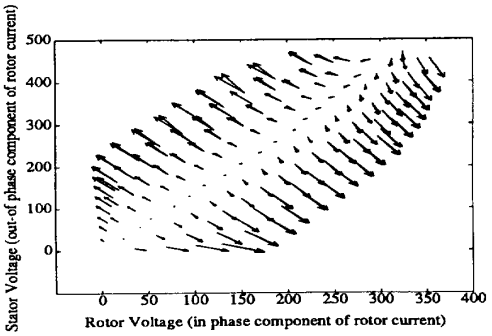

Figure 9: π-model rotor current vectors. Comparison of values predicted by the π-model with measured data. Each data point consists of two vectors originating from the same point. The location of each origin indicates the rotor and stator rms line-to-line voltages, and the vectors indicate the calculated and measured rotor current vectors.

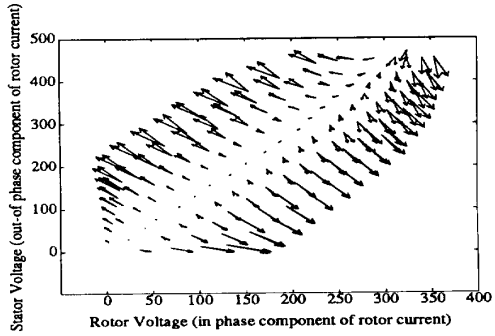

Figure 10: T-model rotor current vectors. Comparison of values predicted by the T-model with measured data. As in Fig. 9.

transition between saturated and unsaturated slopes. This also facilitates the calculations.

To make the approximate calculation assuming sinusoidal MMF distributions, we consider the fundamental component of the flux through one nonlinear reluctance element (made up of parts of many teeth) given a sinusoidal MMF distribution across the element. This is given by

$$\lambda = \int_0^{2\pi} n \sin\theta \, g^{-1}(a \sin\theta) \, d\theta \qquad (11)$$

where λ is the flux linkage in a sinusoidal winding of n peak turns, a is the amplitude of the MMF, and $g^{-1}(\cdot)$ is the characteristic of the nonlinear reluctance element. For $g^{-1}(\cdot)$ piecewise linear with a break point at b, an initial slope of s_1 and a final slope of s_2,

$$\begin{aligned} \lambda &= \pi a s_2 - 2a(s_2 - s_1)\sin^{-1}(b/a) \\ &\quad -2(s_2 - s_1)b\sqrt{1 - b^2/x^2} \end{aligned} \qquad (12)$$

for a greater than b.

Using this form to characterize elements of the vector magnetic circuit, flux linkage vectors were calculated for a

grid of 21 different stator MMF amplitudes, and 21 different rotor MMF amplitudes, both with the vector directions of the MMF's aligned, and with them 90 degrees apart. The calculations were repeated by the more exact method of calculating flux distributions explicitly, and numerically integrating to get the flux linkage. For the purposes of these calculations, arbitrary machine characteristics were assumed: Leakage reluctance was five, unsaturated rotor and stator reluctances were one, going up to ten past the break point of one. MMF amplitudes ranged from zero to four.

The results of these calculations showed that the error introduced by the approximation was small. The maximum percentage error in any one flux vector was 2.64%. The rms of all the percentage errors was 1.04%. It is expected that this roughly represents a worst case for the error this approximation would introduce in any real machine, since teeth in a real machine will have more gradual saturation characteristics.

V. Blondel-Park Transformation

The characteristics of the functions $F_s(\cdot)$ and $F_r(\cdot)$ allow moving a rotation ($e^{-\mathbf{J}\theta}$) inside or outside the function. This is useful because it allows performing the Blondel-Park transformation. We introduce the transformation

$$\begin{bmatrix} \vec{\lambda}_s^x \\ \vec{\lambda}_r^x \end{bmatrix} = T(\theta,\rho) \begin{bmatrix} \vec{\lambda}_s^s \\ \vec{\lambda}_r^r \end{bmatrix} \tag{13}$$

where

$$T(\theta,\rho) = \begin{bmatrix} e^{-\mathbf{J}\rho} & 0 \\ 0 & e^{\mathbf{J}(\theta-\rho)} \end{bmatrix}, \tag{14}$$

and the superscript x indicates an arbitrary reference frame, at an angle ρ from the stator reference frame. Both θ and ρ may be time varying. The electrical dynamics become

$$\begin{bmatrix} \dot{\vec{\lambda}}_s^x \\ \dot{\vec{\lambda}}_r^x \end{bmatrix} = \begin{bmatrix} -\dot{\rho}\,\mathbf{J}\vec{\lambda}_s^x \\ (\dot{\theta}-\dot{\rho})\mathbf{J}\vec{\lambda}_r^x \end{bmatrix} + \begin{bmatrix} \vec{v}_s^x \\ \vec{v}_r^x \end{bmatrix} - \underline{\mathbf{R}} \left\{ \underline{\mathbf{C}}_0 \begin{bmatrix} \vec{\lambda}_s^x \\ \vec{\lambda}_r^x \end{bmatrix} + \begin{bmatrix} F_s(\vec{\lambda}_s^x) \\ F_r(\vec{\lambda}_r^x) \end{bmatrix} \right\}, \tag{15}$$

where $\underline{\mathbf{C}}_0$ is defined by

$$\underline{\mathbf{C}}_0 = \begin{bmatrix} (\frac{1}{L_r}+\frac{1}{L_\ell})\mathbf{I} & -\frac{\mathbf{I}}{L_\ell} \\ -\frac{\mathbf{I}}{L_\ell} & (\frac{1}{L_r}+\frac{1}{L_\ell})\mathbf{I} \end{bmatrix}, \tag{16}$$

$$\begin{bmatrix} \vec{v}_s^x \\ \vec{v}_r^x \end{bmatrix} = T(\theta,\rho) \begin{bmatrix} \vec{v}_s^s \\ \vec{v}_r^r \end{bmatrix}, \tag{17}$$

and $\underline{\mathbf{R}}$ is the 4×4 matrix of stator and rotor resistance. The principle benefit of the transformation is the removal of angular dependence from the dynamics (15), so that the system becomes time-invariant for constant speed $\dot{\theta}$. The transformation can be used to change to any reference frame, by the appropriate choice of ρ. One particularly useful choice of reference is the field-oriented reference frame. Aligning the reference frame with the rotor flux vector simplifies the model because the quadrature component of rotor flux is zero, and so the rotor flux vector can be treated as a scalar quantity. This is used for field-oriented control techniques discussed briefly in Section VIII and in more detail in [7].

We use different superscripts to designate the transformed quantities in different reference frames, summarized in Table II.

TABLE II
REFERENCE FRAME SUPERSCRIPT DESIGNATIONS

superscript designation	reference frame	ρ
s	Stator	$\rho = 0$
r	Rotor	$\rho = \theta$
x	Arbitrary	ρ
e	Field-Oriented	$\angle(\vec{\lambda}_r^r)$

VI. Torque Production

Since many common methods of calculating torque are valid only for linear magnetics, we must take care in calculating torque for the nonlinear-magnetics case. Because our model is flux-controlled it is most straight forward to calculate the torque as a function of flux and angle by differentiating the field energy.[2]

$$\tau(\vec{\lambda}_s^s, \vec{\lambda}_r^r, \theta) = -\frac{\partial W_f(\vec{\lambda}_s^s, \vec{\lambda}_r^r, \theta)}{\partial \theta} \tag{18}$$

We calculate W_f by $\int \vec{\mathbf{i}}^T d\vec{\boldsymbol{\lambda}}$, resulting in

$$W_f = \left[-\frac{1}{L_\ell} e^{\mathbf{J}\theta}\vec{\lambda}_r^r\right]^T \vec{\lambda}_s^s + (\theta\text{-independent terms}) \tag{19}$$

The torque is then

$$\tau(\vec{\lambda}_s^s, \vec{\lambda}_r^r, \theta) = \left[-\frac{1}{L_\ell}\mathbf{J}e^{\mathbf{J}\theta}\vec{\lambda}_r^r\right]^T \vec{\lambda}_s^s \tag{20}$$

or in terms of the Park-transformed flux,

$$\tau(\vec{\lambda}_s^x, \vec{\lambda}_r^x, \theta) = \left[-\frac{1}{L_\ell}\mathbf{J}\vec{\lambda}_r^x\right]^T \vec{\lambda}_s^x = \frac{1}{L_\ell}(\lambda_{sd}^x\lambda_{rq}^x - \lambda_{sq}^x\lambda_{rd}^x) \tag{21}$$

This expression is identical to one form of the expression for the torque with linear magnetics. It can be shown to be equivalent to another common form,

$$\tau = \vec{\imath}_s^{\,x\,T}\mathbf{J}\vec{\lambda}_s^x. \tag{22}$$

[2]We use the convention that torque is positive in the motoring direction.

VII. Steady State Operation in Saturation

One interesting implication of the π-model is that, unlike transformers, smooth air-gap machines with balanced sinusoidal voltage excitation and sinusoidally distributed windings have sinusoidal terminal currents even in heavy saturation. In a transformer the magnitude of the flux changes at the supply frequency, going from saturation in one direction through zero to saturation in the other direction and back. But in the smooth air-gap machine, the flux vector stays at a constant magnitude, and rotates at the supply frequency, and so the current vector does likewise. This constant-magnitude rotating current vector corresponds to sinusoidal phase currents. The model can also be used to show that the waveforms in saturation do not remain sinusoidal with unbalanced sinusoidal excitation [13].

We now consider operation with the rotor shorted, corresponding to a squirrel-cage machine. In steady state operation, with a fixed mechanical speed and torque, there is one degree of freedom that may be adjusted to optimize the efficiency. This is often discussed in terms of finding the optimal slip, but finding the optimal rotor flux is equivalent. Assuming all loss is copper loss, the rotor flux for operation at a given torque with minimal loss is independent of the speed or frequency. For this reason, we approach optimal efficiency operation in terms of finding the optimal rotor flux. Our result is only correct if core loss is negligible. Although core loss often may be neglected in calculating dynamics for such applications as control design, it is more important for efficiency calculations. Nonetheless, the analysis without core loss can be useful in understanding general trends in how a machine performs when driven far into magnetic saturation, and in identifying useful ranges of operation for particular applications.

From a given torque and rotor flux we calculate loss, using the rotor-flux oriented reference frame. From the equations of motion in this frame [7] we find the stator flux,

$$\lambda_{sd}^e = L_\ell \left[(\frac{1}{L_r} + \frac{1}{L_\ell})\lambda_{rd}^e + f_r(\lambda_{rd}^e) \right] \tag{23}$$

and

$$\lambda_{sq}^e = -\tau \frac{L_\ell}{\lambda_{rd}^e}. \tag{24}$$

The stator current is then

$$\vec{i}_s^e = F_s(\vec{\lambda}_s^e) + (\frac{1}{L_s} + \frac{1}{L_\ell})\vec{\lambda}_s^e - \frac{1}{L_\ell} \begin{bmatrix} \lambda_{rd}^e \\ 0 \end{bmatrix}, \tag{25}$$

and similarly the rotor current is

$$\vec{i}_r^e = \begin{bmatrix} f_r(\lambda_{rd}^e) + (\frac{1}{L_s} + \frac{1}{L_\ell})\lambda_{rd}^e \\ 0 \end{bmatrix} - \frac{1}{L_\ell}\vec{\lambda}_s^e \tag{26}$$

where $f_r(\cdot)$ is the scalar version of $F_r(\cdot)$. The loss is

$$P_{loss} = \|i_s\|^2 R_s + \|i_r\|^2 R_r \tag{27}$$

The rotor flux giving a minimum loss can then be found numerically.

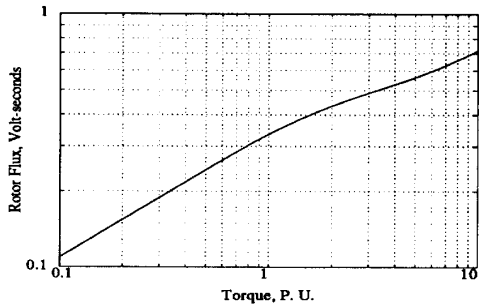

Figure 11: Rotor flux for optimal efficiency operation.

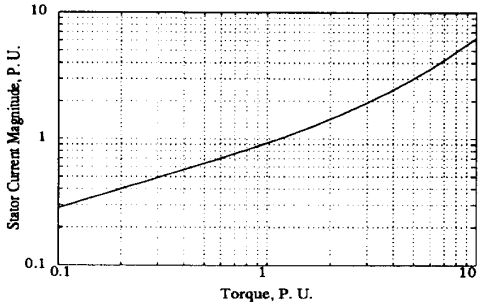

Figure 12: Stator current for optimal efficiency operation.

This optimal rotor flux has been calculated for the experimentally measured machine in Section IV. Torque was calculated from the model as discussed in Section VI. The optimal rotor flux is shown as a function of the calculated torque in Fig. 11. Figs. 12-16 show other calculated parameters as a function of calculated torque. While Figs. 11 and 12 are valid for any speed, for Figs. 13-16 the machine's rated speed of 1800 r/min was assumed.

From these figures, we can see that at ten times rated full load torque, efficiency has dropped to 58%. This is significantly lower than the efficiency between zero and rated torque, 81-82%, but is still usable in some situations. The current required increases rapidly above rated torque,

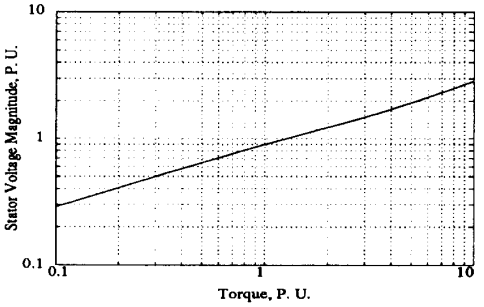

Figure 13: Stator voltage for optimal efficiency operation.

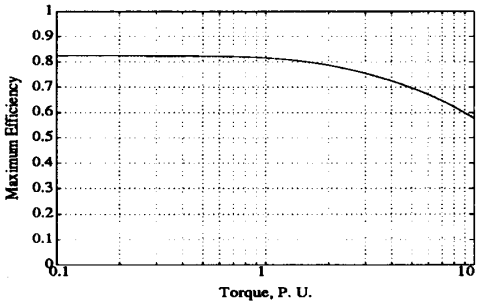

Figure 14: Maximum efficiency as a function of torque.

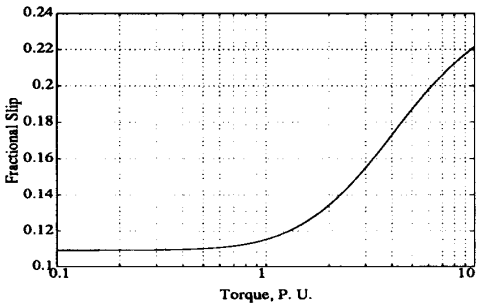

Figure 15: Slip for optimal efficiency operation.

with 6.3 times of rated current required for ten times rated torque. Voltage, however, does not increase as quickly. In fact less voltage is required than would be expected if the machine remained linear at high flux levels. Less than three times rated voltage is needed for ten times rated torque. Furthermore, if the increased torque is required only at lower speeds, the voltage required would be less. Power output per V-A input decreases at high torques, due to decreases in both efficiency and power factor. While the curves shown here are specific to one machine, they give a general idea of the possibilities for operation of any induction machine at torque levels well above its rating, and could be recalculated for any particular machine.

VIII. Field-Oriented Control

In field-oriented control, the use of a reference frame oriented in the direction of the rotor flux vector results in decoupled control of rotor flux and torque [6, 10]. Cross-saturation effects can severely disrupt performance of a control system designed without taking these effects into account [14]. Control systems based on the nonlinear T-model have been developed to mitigate these problems [6, 11, 12, 15]. However, field-oriented control based on the π-model has advantages in simplicity, as well as being more closely based on a physical model of the machine [7].

The equations of motion in the field-oriented reference

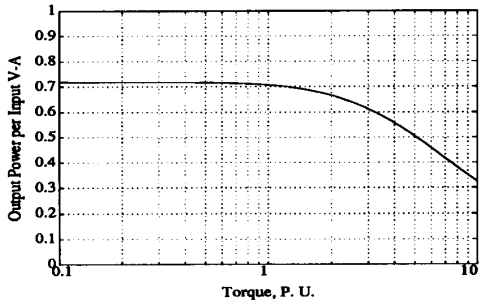

Figure 16: Output power per input V-A in optimal efficiency operation.

frame, with the rotor shorted, are:

$$\dot{\rho} = \frac{R_r}{L_\ell}\frac{\lambda^e_{sq}}{\lambda^e_{rd}} + \dot{\theta}\,. \tag{28}$$

$$\dot{\lambda}^e_{rd} = -R_r\left[\left(\tfrac{1}{L_r}+\tfrac{1}{L_\ell}\right)\lambda^e_{rd} - \tfrac{1}{L_\ell}\lambda^e_{sd} + f_r(\lambda^e_{rd})\right] \tag{29}$$

$$\dot{\vec{\lambda}}^e_s = -\dot{\rho}\,\mathbf{J}\vec{\lambda}^e_s + \vec{v}^e_s - R_s\left\{\left(\tfrac{1}{L_s}+\tfrac{1}{L_\ell}\right)\vec{\lambda}^e_s - \tfrac{1}{L_\ell}\begin{bmatrix}\lambda^e_{rd}\\ 0\end{bmatrix} + F_s(\vec{\lambda}^e_s)\right\} \tag{30}$$

$$\dot{\omega} = \frac{1}{J_{inertia}}\left(-\frac{1}{L_\ell}\lambda^e_{sq}\lambda^e_{rd} - \tau_{load}\right) \tag{31}$$

$$\dot{\theta} = \omega. \tag{32}$$

Conventional field-oriented control often uses a current-source inverter so that the coupling introduced by the linear-magnetics equivalent of (30) is removed. To do this with the nonlinear π-model, which is formulated in terms of flux, one must calculate the current command by

$$\tilde{\vec{i}}^e_s = F_s(\tilde{\vec{\lambda}}^e_s) + \left(\frac{1}{L_s}+\frac{1}{L_\ell}\right)\tilde{\vec{\lambda}}^e_s - \frac{1}{L_\ell}\begin{bmatrix}\lambda^e_{rd}\\ 0\end{bmatrix}, \tag{33}$$

where $\tilde{}$ indicates a commanded value. This calculation removes the cross coupling that would be present if i_{sd} and i_{sq} were used directly to control flux and torque, respectively. A block diagram of such a control system is shown in Fig. 17.

Another option is to control the machine from a voltage-source inverter instead of a current-source inverter. This reintroduces the cross-coupling from (30). However, this coupling can be removed by appropriate compensation in the controller, as has been done for the linear-magnetics case [6, 10, 16]. The controller for a saturated machine can be very similar to the controller for the linear-magnetics case [7].

In order to completely implement a control system based on these methods, a method of measuring or estimating rotor flux is needed. In [7], simulations of a stator-based observer show good performance, except at low frequencies

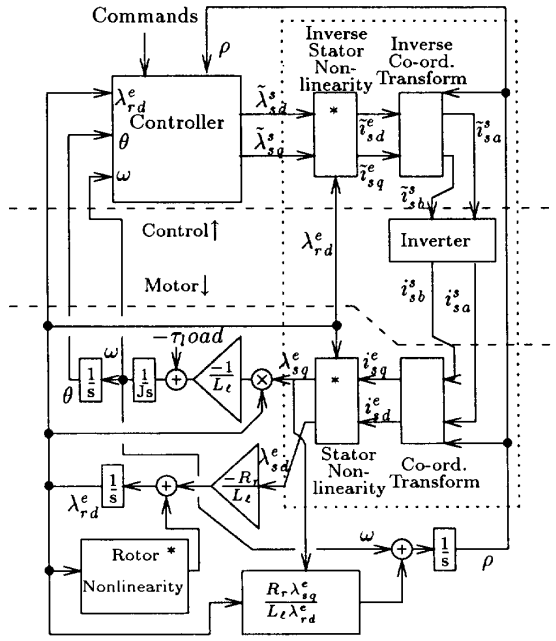

Figure 17: Field oriented control system for magnetically saturating machine. * indicates blocks affected by saturation. Section enclosed by dotted box ideally cancels.

or dc. Thus a different observer is required for a high performance position control system. A simple rotor-based scheme works down to dc, but is adversely affected by rotor resistance variations [7], so more work is needed to develop a robust observer for position control applications.

IX. Conclusion

A new nonlinear π-model of induction machines operating in magnetic saturation has been developed. It is based on a magnetic circuit model of a rotor-stator tooth pair, with two nonlinear elements representing the saturation in the rotor and in the stator. The model of a tooth pair is extended to a model of the machine by assuming an infinite number of infinitesimal teeth. The model is compatible with the Blondel-Park transformation, and so many standard analysis and control methods can be applied. Comparisons with measured data show a slightly better fit for the new nonlinear π-model than for the nonlinear T-model. The π-model is preferred to the T-model because it is more closely based on a physical model of the machine, and because it can be easier to use in simulation and control. Operation with minimal resistive losses has been analyzed as an approximation to optimal efficiency operation in the case that hysteresis and eddy current losses in the iron are small. This analysis shows that operation with torque well aboved rated torque is possible, but does result in lowered efficiency and high stator currents.

References

[1] J. E. Brown, K. P. Kovacs, and P. Vas. A method of including the effects of main flux path saturation in the generalized equations of a.c. machines. *IEEE Transactions on Power Apparatus and Systems*, 102(1):96–103, January 1983.

[2] P. Vas, K. E. Hallenious, and J. E. Brown. Cross-saturation in smooth-air-gap electrical machines. *IEEE Transactions on Energy Conversion*, (1):103–109, March 1986.

[3] Russel J. Kerkman. Steady-state and transient analysis of an induction machine with saturation of the magnetizing branch. *IEEE Transactions on Industry Applications*, 21(1):226–234, January/February 1985.

[4] Jean Robert. A simplified method for the study of saturation in a-c machines. In J. Robert and D. K. Tran, editors, *Modelling and Simulation of Electrical Machines and Power Systems*, pages 129–136. Elsevier Science Publishers B. V., North-Holland, 1988.

[5] M. S. Garrido, L. Pierrat, and E. Dejaeger. The matrix analysis of saturated electrical machines. In J. Robert and D. K. Tran, editors, *Modelling and Simulation of Electrical Machines and Power Systems*, pages 137–144. Elsevier Science Publishers B. V., North-Holland, 1988.

[6] Peter Vas. *Vector Control of AC Machines*. Oxford University Press, 1990.

[7] C. R. Sullivan and S. R. Sanders. Modeling the effects of magnetic saturation on electrical machine control systems. In *Nonlinear Control Systems Design Symposium*. International Federation of Automatic Control, 1992.

[8] Xiaojun Z. Liu, George C. Verghese, and Jeffrey H. Lang. Generalizing the blondel-park transformation of electrical machines: Necessary and sufficiennt conditions:. *IEEE Transactions on Circuits and Systems*, 36(8):1058–1067, August 1989.

[9] M. Vidyasagar. *Nonlinear System Analysis*, chapter 4.1, pages 97–112. Prentice-Hall, 1978.

[10] W. Leonhard. *Control of Electrical Drives*. Springer-Verlag, 1985,1990.

[11] Emil Levi, Slobodan Vukosavic, and Vladan Vuckovic. Saturation compensation schemes for vector controlled induction motor drives. In *PESC '90 Record*, pages 591–598, 1990.

[12] E. Levi and V. Vuckovic. Field-oriented control of induction machines in the presence of magnetic saturation. *Electric Machines and Power Systems*, 16(2):133–147, 1989.

[13] Charles R. Sullivan. Master's thesis, University of California, Berkeley, in progress.

[14] P. Vas and M. Alakula. Field-oriented control of saturated induction machines. *IEEE Transactions on Energy Conversion*, 5(1):218–223, March 1990.

[15] Zbigniew Krzeminski. Differential equations of induction motor with nonlinear control synthesis with regard to saturation of main magnetic path. *Rozprawy Elektrotechniczne*, 34(1):117–131, 1988.

[16] J. M. D. Murphy and F. G. Turnbull. *Power Electronic Control of AC Motors*. Pergamon Press, 1988.